The International Journal of Advanced Manufacturing Technology (2024) 133:3011–3022
https://doi.org/10.1007/s00170-024-13930-z

ORIGINAL ARTICLE

Identification of forming performance parameters for 6016 aluminum alloy sheet under different strain paths via digital image correlation technology

Ziyun Huang[1] · Shun Liu[1] · Sun jin[1] · Shuhui Li[1]

Received: 6 December 2023 / Accepted: 27 May 2024 / Published online: 12 June 2024

Abstract
Aluminum alloys, known for their effective weight reduction, are widely used in the automotive industry. However, compared to steel, they exhibit challenges such as lower room-temperature elongation rates, inferior plasticity, and a higher tendency to crack during forming processes, which significantly limits their application. The current investigation aims to comprehensively investigate the mechanical properties and forming characteristics of 6016 aluminum alloy sheets. Specifically, Digital Image Correlation (DIC) technology was employed to conduct tensile tests on the sheets under various strain paths, including uniaxial tension, shear, and plane strain. Initially, the tests focused on evaluating the mechanical properties and forming characteristics of the aluminum alloy sheets. Subsequently, stress–strain relationship models were established, with results indicating that the saturated stress–strain models, exemplified by the Voce model, are more suitable. Furthermore, this study analyzed the critical failure states of the 6016 aluminum alloy sheets under different strain paths and measured the critical thickness at necking and fracture. These findings provide significant insights for evaluating the failure of aluminum alloy sheets post-forming.

Keywords 6016 aluminum alloy · Digital image correlation · Forming properties · Different strain paths

1 Introduction

Lightweighting is one of the most crucial development directions in the modern automotive industry [1–3] and serves as a key method to effectively reduce vehicle fuel consumption [4–6]. Replacing steel with aluminum alloy for structural and exterior components can reduce vehicle weight by over 40% and decrease fuel consumption by 30% [7]. In the production of auto panels, stamping is the most widely used forming process [8, 9]. However, aluminum alloy sheets, compared to steel, face challenges such as inferior stamping performance and the inapplicability of existing, more mature stamping molds and process design experience [10–13], significantly limiting their application in the industrial production of auto panels [14, 15]. Moreover, the complex shapes of auto panels add significant intricacy to the strain paths during forming [16]. Consequently, an exhaustive investigation into the mechanical properties and formability of aluminum alloy sheets is imperative, offering crucial insights for finite element simulation and practical engineering implementations in forming operations.

Numerous researchers have already conducted studies on the mechanical properties and forming characteristics of aluminum alloys [17], with uniaxial tensile tests being the most widely applied. Researchers typically focus on the effects of varying strain rates, deformation temperatures, and material microstructures on the mechanical properties [18–20]. Neto et al. [21] analyzed the heat generated by plastic deformation in AA6016 aluminum alloy during quasi-static uniaxial tensile tests at different stretching speeds. Additionally, Shen et al. [22] performed uniaxial tensile tests on 6061 aluminum alloy at various strain rates and developed a modified J–C model. Zhang et al. [23] revealed the mechanical property changes in AA6082 aluminum alloy caused by non-uniform temperature distribution. Lu et al. [24] investigated the thermomechanical properties of 7075 aluminum alloy, finding that the temperature increase due to plastic deformation significantly rose with increasing strain. Xiao et al. [25] studied

✉ Shuhui Li
lishuhui@sjtu.edu.cn

[1] School of Mechanical Engineering, Shanghai Jiao Tong University, Shanghai 200240, China

the thermoformability of AA7075 aluminum alloy, noting that formability improved with decreasing deformation temperature and increasing strain rate under thermal stamping conditions. In terms of low-temperature forming, Yan et al. [26] explored the tensile behavior of 6061 aluminum alloy under low temperatures, discovering that reducing the temperature from 20°C to -80°C effectively enhanced its mechanical properties. Moreover, Bagheri et al. [27] examined the impact of different welding methods on the mechanical and forming behaviors of AA6061 alloy, identifying more optimal welding techniques and parameters. Thirathipviwat et al. [28] studied the structural evolution and dislocation density changes in aluminum-magnesium alloys during uniaxial tensile deformation from a microscopic perspective.

As DIC technology continues to advance in terms of algorithms, speed, scale, and dimensions, its application in material performance testing has gained widespread acceptance and use [29–32]. Deng et al. [33] utilized DIC technology to measure the stress–strain curve of aluminum alloy sheets under various strain rate conditions, thereby analyzing their high-speed forming performance. Liu [34] utilized DIC technology to measure the deformation field on the surface of aluminum alloy specimens under uniaxial tension, thus analyzing the variations of stress and strain during necking. Based on this, Fang et al. [35] proposed an experimental method to improve the accuracy of DIC technology in detecting local necking of specimens. In addition, numerous researchers have proposed innovative methods for applying DIC technology to uniaxial tensile tests. Jordan et al. [36] introduced the idea of using surround DIC to obtain precise strain measurements of specimens, reducing the measurement errors of stress–strain curves. Li et al. [37] presented a method for rapidly obtaining the stress–strain curve of metal sheets within a large strain range utilizing DIC technology.

In summary, current research on the mechanical properties and forming characteristics of aluminum alloy sheets is predominantly based on uniaxial tensile tests. However, in the actual production process of auto panels, aluminum alloy sheets undergo complex and varied strain states, making uniaxial tensile testing insufficient for comprehensive analysis. This study innovates by employing DIC technology to conduct tensile tests on the 6016 aluminum alloy sheets under various strain paths, including uniaxial tension, shear, and plane strain. This approach allows for a more thorough elucidation of the mechanical properties and forming characteristics. This study accomplishes an in-depth investigation of mechanical properties, the development of stress–strain relationship models, and an analysis of critical failure states under different strain paths. These findings provide crucial data and monitoring basis for finite element simulation of the forming process and the actual forming operation of the 6016 aluminum alloy sheets.

2 Experiments

2.1 Material and specimens

The material applied for this experiment was 1mm-thick 6016-T4 aluminum alloy sheet, which are widely utilized in the manufacturing of auto panels.

The ASTM E8 standard specimen is adopted for uniaxial tension test, shown in Fig. 1(a). The simple shear specimen designed by Peirs et al. [38] is adopted for shear test, shown in Fig. 1(b). The dimensions of the selected plane strain test specimen are shown in Fig. 1(c), the effectiveness of this specimen will be validated in Sect. 5.2.

The preparation of the specimens requires a series of operations. The basic process used in this experiment is as follows:

(1) Cutting: Utilizing a wire cutting machine, specimens were cut from the sheets in three directions: 0°, 45°, and 90°, relative to the rolling direction of the material.
(2) Numbering: Group the specimens and assign their numbers based on the angle.
(3) Cleaning: Utilize alcohol to wipe the surface of the specimens to remove any residual oil stains from the machining process.
(4) Painting: First, spray white primer on the region of interest for strain analysis. Then, spray black point paint on that area to facilitate strain measurement using DIC technology.
(5) Drying: Allow the painted specimens to dry.

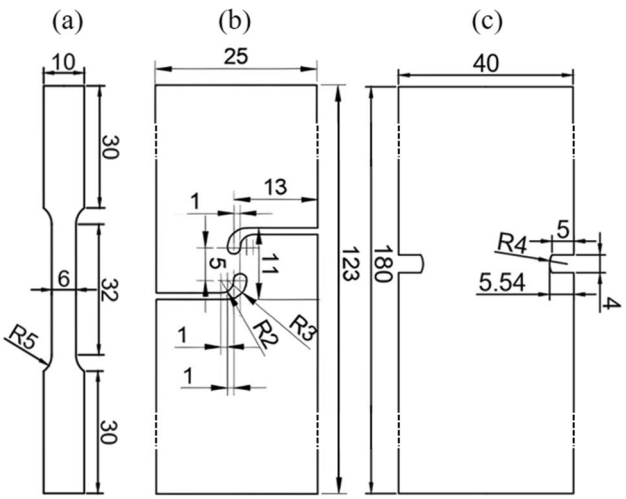

Fig. 1 Specimen dimensions (unit: mm) (**a**) in-plane uniaxial tensile test specimen (UTT-specimen), (**b**) in-plane shear test specimen (ST-specimen) and (**c**) in-plane plane strain test specimen (PST-specimen)

2.2 Experimental setup

The tensile testing machine utilized in this experiment was the Zwick/Roell Z100 universal electronic testing machine from Germany, with a maximum testing force of 100kN and a beam speed range of 0.0001 to 1500mm/min. The DIC testing system utilized was the GOM Aramis 4M system from Germany, as shown in Fig. 2. During the test, to ensure that the specimen undergoes quasi-static deformation during the tensile process, a tensile speed of 1.5 mm/min was set. In the DIC testing system, strain analysis areas for each specimen were selected. By tracking the positional changes of pixel points before and after deformation, the strain fields within these analysis areas were obtained. These were then analyzed using post-processing software, as shown in Fig. 3. Concurrently, tensile force values were acquired from the built-in force sensor of the Zwick/Roell Z100 for subsequent analysis.

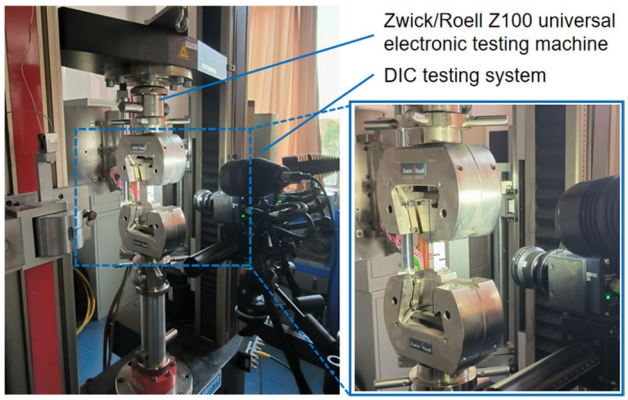

Fig. 2 The experimental setup

3 Mechanical properties study

Compared to the traditional steel sheets commonly used in the auto panel production industry, aluminum alloy sheets have poorer plasticity and are prone to cracking during stamping forming, which poses difficulties for the control of forming quality. In this chapter, the mechanical performance of the 6016 aluminum alloy sheets was analyzed utilizing uniaxial tensile tests. The relationship between various mechanical properties and the forming performance of the sheets was discussed. Furthermore, accurate parameters for the finite element simulation of the forming process were provided.

3.1 Basic mechanical properties study

The uniaxial tensile test was utilized to analyze the basic mechanical properties of the 6016 aluminum alloy sheets. The strain values in the strain analysis area were measured utilizing DIC technology. Simultaneously, the tensile force values were obtained from the force sensor of the tensile testing machine. The engineering stress–strain curve was plotted, as shown in Fig. 4.

The engineering stress–strain curves of individual specimens at the same angle overlap well before fracture. However, there is significant variability in elongation, with the most pronounced difference observed at 90°. The maximum difference in elongation between different specimens is approximately 6%. This is attributed to factors such as non-uniform microstructural defects within the aluminum alloy sheets, which is a normal experimental phenomenon. The basic mechanical property data in the 0°, 45°, and 90° directions relative to the rolling direction are shown in Table 1. The 6016 aluminum

Fig. 3 Analysis steps of DIC testing system

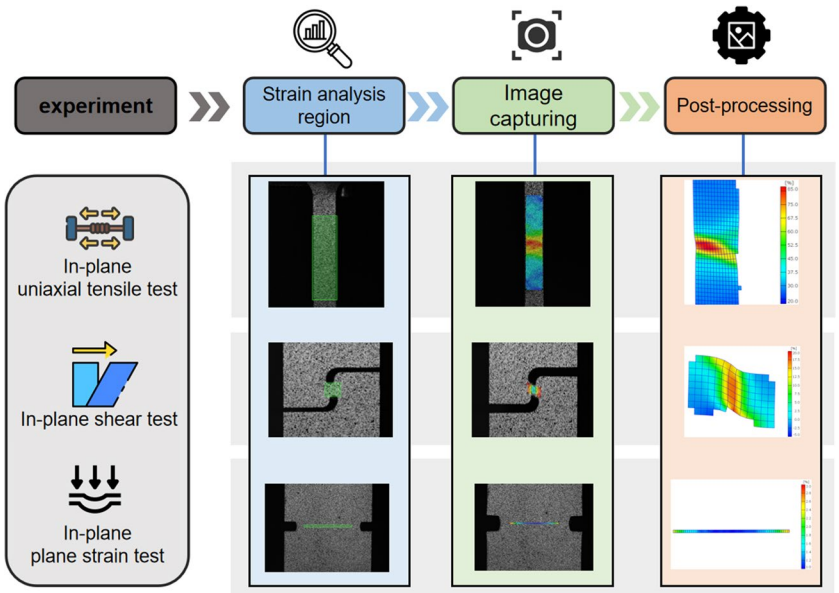

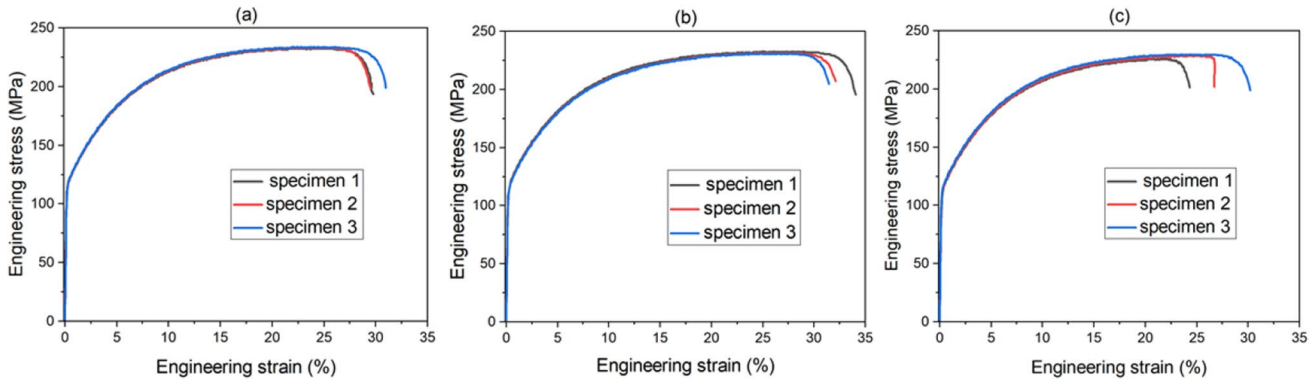

Fig. 4 Engineering stress–strain curves (**a**) 0°, (**b**) 45°, and (**c**) 90°

alloy sheets exhibit similar values of Young's modulus, yield strength, and tensile strength in the three directions. These three mechanical performance parameters show a slight decrease as the angle with the rolling direction increases. The maximum differences between Young's modulus, yield strength, and tensile strength among different angles are 1722 MPa, 3 MPa, and 5 MPa, respectively. The sheets also have a relatively small yield ratio, indicating a longer stage of uniform plastic deformation from the onset of yielding to the point of fracture. This characteristic reduces the likelihood of failure due to cracking in auto panels during the production process and is beneficial for forming processes.

3.2 Hardening characteristics analysis

The study of hardening characteristics is of great significance for evaluating the processing performance of metal materials. Among them, the strain hardening exponent is commonly used to assess the hardening behavior of materials during cold deformation processes [39]. To study the hardening characteristics of the 6016 aluminum alloy sheets, it is necessary to convert the engineering stress–strain curve into true stress–strain curves. Within the range of uniform plastic deformation between the yield point and the necking point, the conversion from engineering stress and engineering strain to true stress and true strain is based on the following equations [40]:

$$e = \Delta L/L_0 \tag{1}$$

$$\varepsilon = \ln(L_i/L_0) = \ln(1+e) \tag{2}$$

$$\sigma = F/A = \sigma_{eng}(1+e) \tag{3}$$

where e is the engineering strain, ΔL is the incremental length of the specimen's test area, L_0 is the initial length of the test area. ε is the true strain, L_i is the length of the specimen after deformation. σ is the true stress, σ_{eng} is the engineering stress, F is the current tensile force, and A is the current cross-sectional area of the specimen.

The specimen from each direction with mechanical property data closest to the average was selected as the calibration specimen for the true stress–strain curve. Plot the true stress–strain curve within the range of uniform plastic deformation after the yield point and before the necking point, as shown in Fig. 5. The true stress–strain curves of the 6016 aluminum alloy sheets in three directions show a high degree of overlap, indicating that the differences in material properties across the plane of the sheet are minimal, and it can be approximately considered isotropic within the plane. Additionally, the true stress–strain curves of the 6016 aluminum alloy sheets are relatively smooth and even, which is beneficial for surface quality control of aluminum alloy stamping parts. Therefore, it is suitable for manufacturing auto panels that have high requirements for surface quality.

The strain hardening index "n" represents the material's ability to undergo work hardening, and it can be obtained by fitting the true stress–strain curve using the hardening relationship equation [40]:

$$\sigma = k\varepsilon^n \tag{4}$$

where σ is the true stress, k is the strength coefficient, ε is the true strain, and n is the strain hardening exponent. Within

Table 1 Mechanical properties of 6016 aluminum alloy sheets

Angle (°)	Young's modulus(MPa)	Yield strength(MPa)	Tensile strength(MPa)	Elongation (%)	Yield ratio
0	67,571	119	233	30.0	0.512
45	66,840	118	232	32.5	0.508
90	65,849	116	228	27.0	0.510

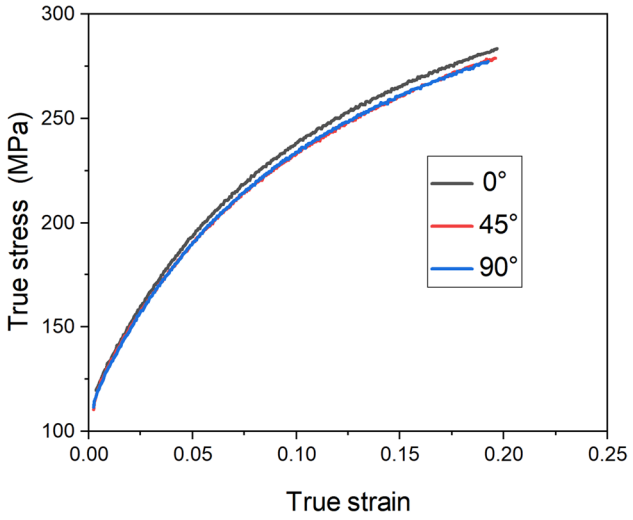

Fig. 5 True stress–strain curves

the range of uniform plastic deformation of the specimen, all strain data points were fitted using the least squares method, and the results are shown in Table 2. The results indicate that the 6016 aluminum alloy sheets have a high strain hardening index, allowing for more uniform deformation under uniaxial stress conditions, with a reduced tendency for strain localization. This contributes to their excellent forming performance and corroborates their characteristic of having a high elongation.

Furthermore, this study investigated the hardening behavior of the 6016 aluminum alloy sheets after baking. Baking hardening is a common metal processing technique that has been widely used in the manufacturing and processing of various alloys. This technique can improve the strength and hardness of aluminum alloys. During the industrial production of auto panels, aluminum alloy sheets undergo temperature changes in the painting and baking process after stamping, which alters the mechanical properties of the material. This makes the mechanical behavior more complex and poses challenges to a comprehensive assessment of stamping formability. Therefore, accurately describing the changes in mechanical properties of pre-strained 6016 aluminum alloy sheets after bake hardening is a critical issue that urgently needs to be addressed for their application in the production of auto panels.

To investigate the effects of various pre-strains and baking hardening on the mechanical properties of the 6016 aluminum alloy sheets, this experiment conducted baking and uniaxial tensile tests on specimens with different pre-strains and angles, as shown in Table 3. The variations in yield strength and tensile strength under different pre-strains were analyzed. The baking conditions were consistent with those in the industrial production of auto panels, with a baking temperature of 170 °C and a baking time of 20 min. The baking process was performed using a Memmert UF110 constant-temperature oven. Once the temperature inside the oven reached and stabilized at 170 °C, the uniaxial tensile specimens were placed inside and left to wait until the temperature reached 170 °C again and stabilized. After a 20-min insulation period, the specimens were removed and cooled to room temperature.

The engineering stress–strain curves under different pre-strain conditions after baking were plotted in Fig. 6. This was done to investigate the influence of different pre-strain and baking hardening on the mechanical properties of the 6016 aluminum alloy sheets and to compare the differences in yield strength and tensile strength.

The results show that both the yield strength and tensile strength significantly increased after baking compared to the original state. Furthermore, the increase was more pronounced with higher levels of pre-strain, as shown in Table 4 and Table 5. Taking the 0° direction as an example, after 12% pre-strain and baking, the yield strength and tensile strength increased by 94.1% and 19.8%, respectively, compared to the original state. The increase in yield strength is more significant. The microstructural explanation for this is that the baking process promotes the precipitation of strengthening phases β'' in the aluminum alloy sheets, thereby improving their mechanical properties [41]. Additionally, the introduction of pre-strain generates a certain amount of dislocations, and as the amount of pre-strain increases, the density of dislocations also increases [42]. Therefore, the increase in yield strength and tensile strength of the sheets is greater with higher levels of pre-strain.

3.3 Analysis of anisotropic properties

Understanding the anisotropy of the 6016 aluminum alloy sheets is essential for achieving finite element simulation of the forming process. For the design of auto panels, the presence of anisotropy can lead to asymmetric forces acting on the structure in different directions, making it more

Table 2 The value of *n*

Angle (°)	0	45	90
n	0.265	0.265	0.260

Table 3 Baking hardening experimental design

Baking conditions	Pre-strain	Angle
170 °C, 20min	0%	0°、45°、90°
	4%	
	8%	
	12%	

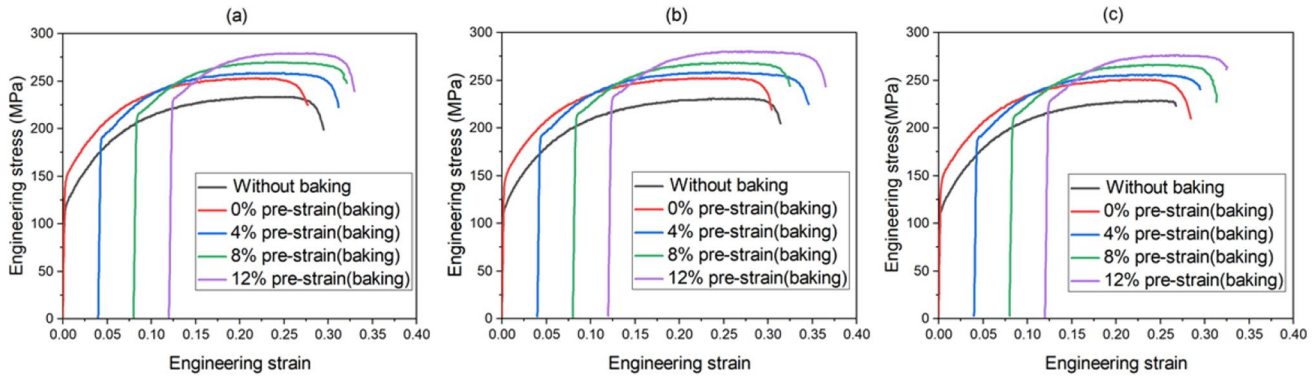

Fig. 6 Engineering stress–strain curves before and after baking (**a**) 0°, (**b**) 45°, and (**c**) 90°

Table 4 The change in yield strength

Angle (°)	Original state (MPa)	0% pre-strain (MPa)	4% pre-strain (MPa)	8% pre-strain (MPa)	12% pre-strain (MPa)
0	119	149	192	215	231
45	118	148	191	213	232
90	116	152	189	212	228

Table 5 The change in tensile strength

Angle (°)	Original state (MPa)	0% pre-strain (MPa)	4% pre-strain (MPa)	8% pre-strain (MPa)	12% pre-strain (MPa)
0	233	253	258	270	279
45	232	252	258	268	280
90	228	250	256	265	276

susceptible to damage or failure. The anisotropic properties of the sheets in the thickness direction can be characterized using the R-value, which can be determined from [40]:

$$R = \frac{\varepsilon_w}{\varepsilon_t} \tag{5}$$

where ε_w is the strain in the width direction of the UTT-specimen, and ε_t is the strain in the thickness direction of the UTT-specimen. Assuming that the test area of the specimen maintains constant volume during the tensile process, an approximation can be made:

$$\varepsilon_g + \varepsilon_w + \varepsilon_t = 0 \tag{6}$$

where ε_g is the strain in the length direction of the UTT-specimen. The values of ε_g and ε_w are obtained through the utilization of DIC technology, followed by subjecting them to linear regression analysis. Noting the slope of the fitted line as m, then R can be determined from substituting m into Eq. 6:

$$R = -\frac{1}{m_r + 1} \tag{7}$$

the value of R in three directions can be derived, which are labeled as R_0、 R_{45} and R_{90}. Then, the average thickness anisotropy coefficient R_{avg} and the planar anisotropy coefficient ΔR can be determined from:

$$R_{avg} = \frac{R_0 + 2R_{45} + R_{90}}{4} \tag{8}$$

$$\Delta R = \frac{R_0 - 2R_{45} + R_{90}}{2} \tag{9}$$

R_{avg} can be used to characterize the deformation ability of the sheet in the thickness direction. A larger R_{avg} indicates that the sheet is more difficult to deform in the thickness direction, which is advantageous for deep drawing processes. On the other hand,ΔR represents the uniformity of deformation within the plane of the sheet. A smaller ΔR indicates that the strain differences in different directions within the plane of the sheet are smaller, resulting in higher uniformity of stretching deformation, which is favorable for deep drawing in stamping processes. Based on the experimental results shown in Table 6, the R-values of the 6016 aluminum alloy sheets vary significantly in different directions, with the highest R-value in the 0° direction and the lowest in the 90°direction, resulting in a difference of 0.25. The value of R_{avg} and ΔR are 0.55 and 0.20. A relatively small ΔR indicates that the in-plane anisotropy can be neglected, which is consistent with the conclusion obtained from Fig. 5.

4 Construction of stress–strain relationship model

The stress–strain relationship model, i.e., strain-hardening equation, is used to characterize the variation of true stress with true strain in materials. It is one of the fundamental models for describing the mechanical properties of materials and is particularly important for the study and application of

Table 6 The value of R

Angle (°)	0	45	90
R	0.70	0.45	0.60

automotive aluminum alloy sheets. Currently, these models are widely used in strength prediction and forming simulations of automotive aluminum alloy sheets.

The strain-hardening equations have been classified into two categories: saturated and unsaturated. In the following section, the differences between the two types of models will be illustrated by using the Hollomon model and the Voce model as representatives, and exploring which type of model is more suitable.

4.1 The hollomon model and the voce model

This section focuses on fitting the true stress–strain curve obtained from the uniaxial tensile tests. The objective is to construct the Hollomon model and the Voce model, and to compare the fitting results of these two models.

The Hollomon model has been described in Sect. 3.2 [43], the stress–strain fitting equation is shown in Eq. 4, and the fitting results for n are presented in Table 2. The fitting results for K are shown in Table 7.

The stress–strain fitting equation for the Voce model is as follows[44]:

$$\sigma = A + B(1 - e^{-C\varepsilon}) \tag{10}$$

where σ is the true stress, ε is the true strain, A、B、C are the undetermined parameters. The fitting results for the model are shown in Table 8.

The stress–strain curves obtained by fitting the Hollomon model and the Voce model in three directions are compared with the true stress–strain curve during the uniaxial tensile tests, as shown in Fig. 7. Within the strain range involved in the uniaxial tensile tests, where the true strain is less than 0.25, both the Hollomon model and the Voce model exhibit a high degree of overlap with the experimental curve, indicating a good fitting effect. However, the stress–strain curve obtained by the Voce model exhibits an even higher degree of overlap with the experimental curve, making it more suitable for constructing the stress–strain relationship model for the 6016 aluminum alloy sheets within this strain range.

4.2 Comparison of fitting effects within a larger strain range

In the shear test, the sheet can generate a larger strain compared to uniaxial tensile test. Therefore, the true stress–strain curve obtained from shear test can be used to validate and compare the fitting effects of the Hollomon model and the Voce model within a larger strain range.

During the experimental process, the average shear angle of the shear zone in the ST-specimen was measured utilizing DIC technology. The tangent of the shear angle was then calculated to obtain the shear strain. The shear stress can be determined from:

$$\tau = \frac{F}{l_0 \cdot t_0} \tag{11}$$

where F is the applied tensile force on the specimen, l_0 is the initial length of the shear zone, and t_0 is the initial thickness of the ST-specimen.

When the sheet is in a shear state, the shear strain and shear stress can be converted to uniaxial tensile strain and stress using the following equation [40]:

$$\varepsilon = e/\sqrt{3} \tag{12}$$

$$\sigma = \tau \cdot \sqrt{3} \tag{13}$$

where ε is the uniaxial tensile strain, e is shear strain, σ is uniaxial tensile stress, and τ is shear stress. This converts the shear stress–strain curves into the uniaxial tensile true stress–strain curves. Using this curve, the fitting effectiveness of the Hollomon model and the Voce model for the 6016 aluminum alloy sheets obtained from the uniaxial tensile test are verified and compared within a large strain range, as shown in Fig. 8. Within the strain range involved in the shear test, i.e., true strain less than 0.6, the stress values of the 6016 aluminum alloy sheets gradually approach a stable value as the strain increases, and the stress–strain curve becomes flat. Therefore, the saturated models represented by the Voce model are more suitable for the stress–strain relationship model of the 6016 aluminum alloy sheets, whereas the unsaturated models represented by the Hollomon model show continuously increasing stress values with increasing strain, without reaching a saturated state. This is inconsistent with the stress–strain change law of aluminum alloys, and

Table 7 Hollomon model k-value fitting results

Angle (°)	K (MPa)
0	435.3
45	428.8
90	425.4

Table 8 Fitting results of the voce model

Angle (°)	A (MPa)	B (MPa)	C
0	116.2	190.5	10.3
45	116.4	189.3	9.7
90	114.9	187.8	10.1

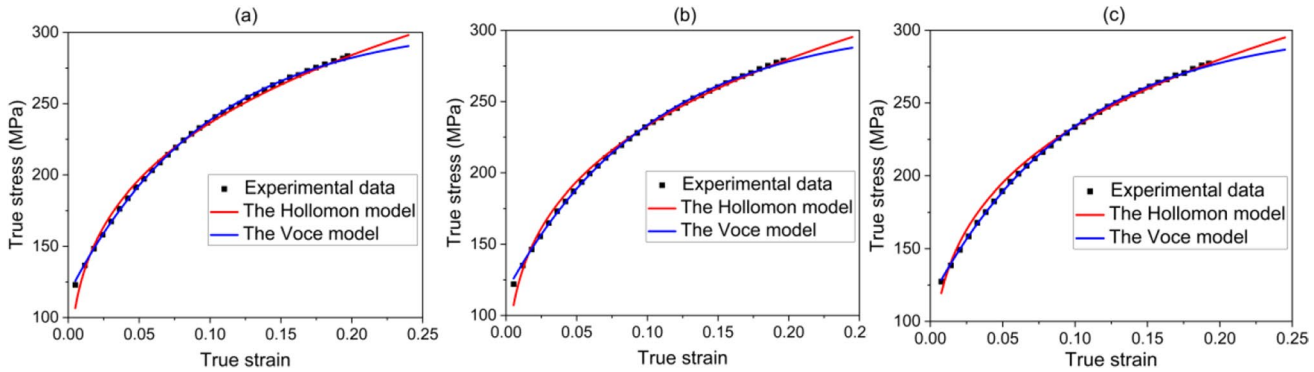

Fig. 7 Comparison of fitting effects (**a**) 0°, (**b**) 45° and (**c**) 90°

the fitting curve of the unsaturated model cannot overlap with the experimental curve within a large strain range, making it unsuitable for the stress–strain relationship model of the 6016 aluminum alloy sheets.

The reason why the Voce model curve does not completely overlap with the experimental curve is that, in the shear zone of the ST-specimen, there are still small amounts of other forms of strain paths besides shear strain. Additionally, as the shear strain increases, the length of the shear zone also undergoes slight changes. Therefore, within the allowed error range of the experiment, it can be approximately assumed that the two curves overlap.

To further enhance the model's ability to fit true stress–strain curves, the Voce model was improved to a combined Voce + Voce model, enhancing the model's fitting effectiveness by increasing the number of parameters to be determined. The stress–strain fitting formula for the Voce + Voce model is presented in the following equation:

$$\sigma = A + B(1 - e^{-C\varepsilon}) + D(1 - e^{-E\varepsilon}) \tag{14}$$

where σ is the true stress, ε is the true strain, A、B、C、D、E are the undetermined parameters. The fitting results for the model are shown in Table 9.

The fitting curves of the Voce + Voce model in three directions are compared with the true stress–strain curves, with the results shown in Fig. 9. The stress–strain curves obtained through the Voce + Voce model fitting closely align with the true stress–strain curves, achieving the intended improvement in fitting accuracy also enables precise prediction of the stress–strain relationship within a larger range of strains. Furthermore, the fitted curves exhibit a smoother profile compared to the experimental curves, which, to a certain extent, mitigates the impact of factors like vibrations at the gripping ends of the tensile machine during the testing process.

5 Analysis of critical failure state for different strain paths

The significance of studying the critical failure states under different strain paths of aluminum alloy sheets lies in gaining a deeper understanding of their mechanical properties and failure mechanisms under various strain conditions. In the plastic processing of aluminum alloys, failure behavior mainly includes phenomena such as necking, fracture, and

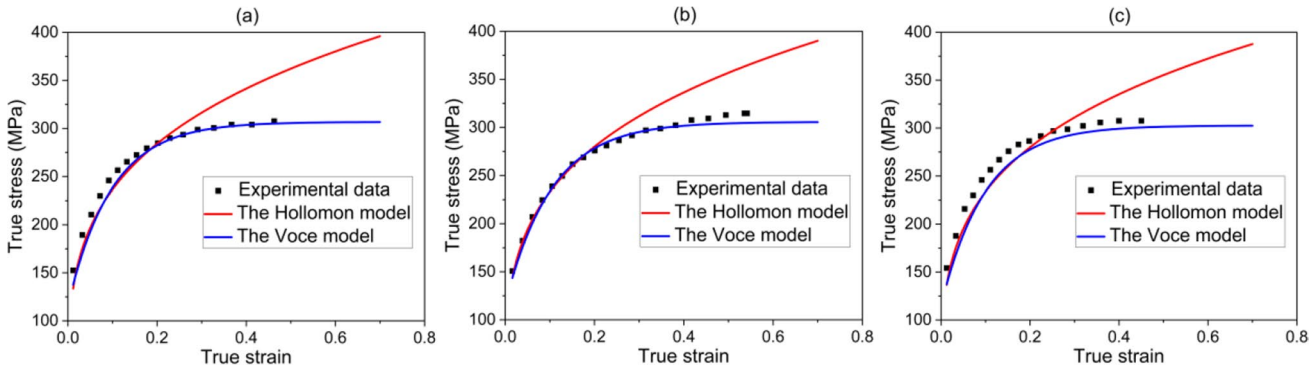

Fig. 8 Comparison of fitting effects within a larger strain range (**a**) 0°, (**b**) 45°, and (**c**) 90°

Table 9 Fitting results of the Voce + Voce model

Angle (°)	A (MPa)	B (MPa)	C	D (MPa)	E
0	129.3	104.2	17.1	79.3	6.0
45	124.1	108.0	15.2	102.1	3.2
90	127.9	61.4	21.6	121.1	8.4

crack propagation, all of which are influenced by the strain path. By studying the critical failure state under different strain paths, it is possible to evaluate the crack resistance and deformation characteristics of the 6016 aluminum alloy sheets during plastic processing, and to reveal the failure mechanisms and inherent differences of the 6016 aluminum alloy sheets under different strain paths.

5.1 Critical thickness measurement of uniaxial tensile strain state

In the actual use of aluminum alloy sheet, when necking occurs, although the cross-section of the component has not yet fractured, it begins to shrink rapidly, and there are hidden defects in the component. Therefore, the occurrence of necking represents the failure of auto panels. The critical thickness of the failure of auto panels can be characterized by the thickness of the aluminum alloy sheet at the onset of necking. The onset of necking can be determined using the strain rate curve, as shown in Fig. 10.

Utilizing DIC technology, the thinning rate of the thickness at the onset of necking was observed and measured during the uniaxial tensile test. The results are shown in Table 10. The average thickness at the onset of necking for UTT-specimens in three directions ranges from 0.80 to 0.85mm, yet there is significant data fluctuation, resulting in considerable variability in the thickness reduction rate at the onset of necking for each direction of the UTT-specimens.

In addition, utilizing DIC technology, the fracture thickness of the UTT-specimens was measured at the moment of fracture. This provides valuable reference information for the actual production and use of aluminum alloy auto panels under uniaxial tensile conditions. The results are shown in Table 11. The results indicate that the average thickness at fracture ranged from 0.63 to 0.65mm.

5.2 Critical thickness measurement of plane strain state

Plane strain test is also a common method in material mechanics, mainly used to study the failure and forming limit characteristics of materials under plane strain. During the tensile process of PST-specimen, the DIC technology was utilize to measure the major and minor strain data in the concentrated plane strain region. Based on this, the logarithmic major strain and logarithmic minor strain curves are plotted as a function of time (taking sample 1 in the 0° direction as an example), as shown in Fig. 11. The horizontal axis

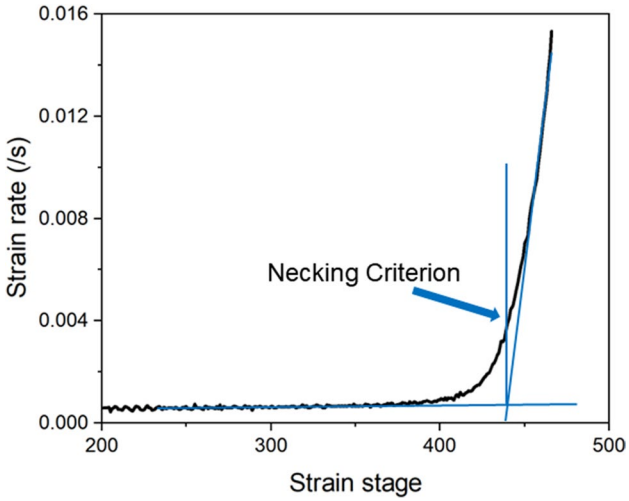

Fig. 10 Method for determining the onset of necking

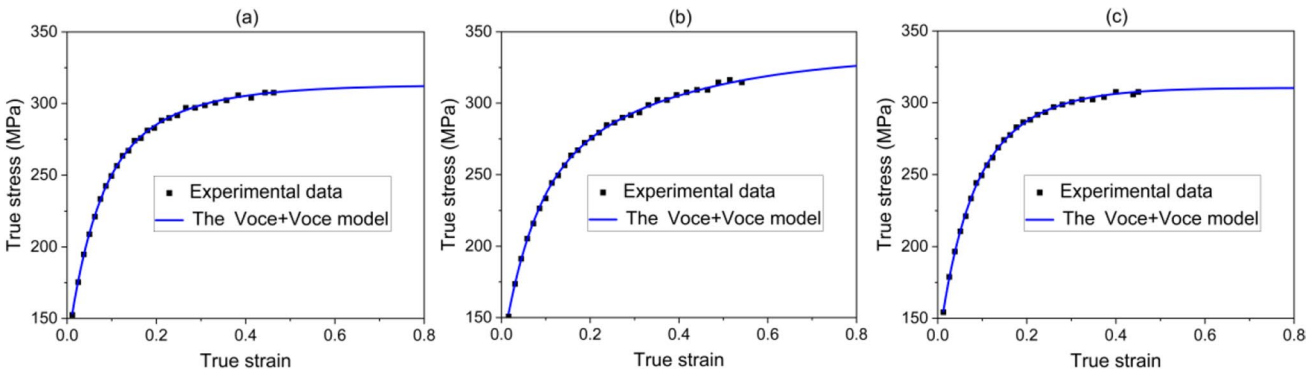

Fig. 9 Fitting effect of the Voce + Voce Model (**a**) 0°, (**b**) 45° and (**c**) 90°

Table 10 Thickness of the UTT-specimens at the onset of necking

Angle (°)	Thickness Reduction rate (%)	Thickness (mm)
0	15.59	0.8441
45	19.80	0.8020
90	16.38	0.8362

Table 11 Thickness of the UTT-specimens at the onset of fracture

Angle (°)	Thickness Reduction rate (%)	Thickness (mm)
0	35.21	0.6479
45	36.25	0.6375
90	36.05	0.6395

t/t_{max} represents the normalized time parameter, t represents the current testing time, and t_{max} represents the fracture time of the PST-specimen.

During the loading process of the PST-specimen until fracture, the major strain increased continuously with time, while the minor strain remained approximately zero throughout this process, which can be neglected compared to the major strain. This phenomenon indicates that the principal strain path in the concentrated plane strain region of the PST-specimen is plane strain, confirming the reliability of the experiment.

The method used in Sect. 5.1 was employed to determine the onset of necking in the PST-specimens. The thinning rates of the specimen were measured, and the results are presented in Table 12. The experimental data for the thickness at the onset of necking in the PST-specimens in different directions exhibit high consistency. The average thickness at the onset of necking ranges from 0.79 to 0.81mm.

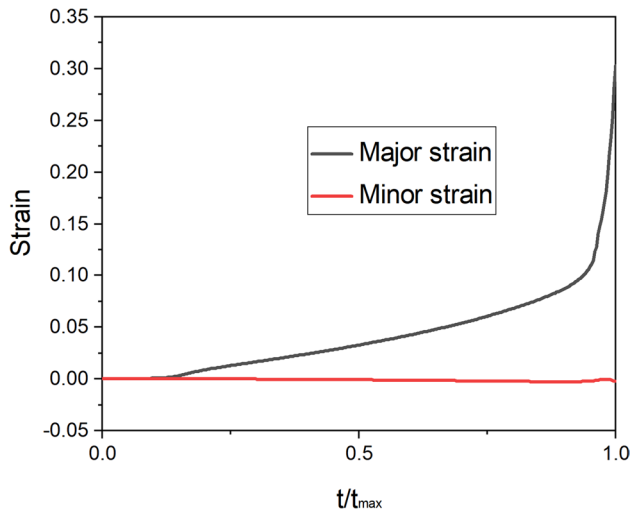

Fig. 11 Major and minor strain of the PST-specimen

Table 12 Thickness of the PST-specimens at the onset of necking

Angle (°)	Thickness Reduction rate (%)	Thickness (mm)
0	19.09	0.8091
45	20.92	0.7908
90	19.31	0.8069

Table 13 Thickness of the PST-specimens at the onset of fracture

Angle (°)	Thickness Reduction rate (%)	Thickness (mm)
0	34.04	0.6596
45	34.97	0.6503
90	34.95	0.6505

The fracture thickness of the PST-specimens was measured utilizing the DIC technology to obtain the maximum thickness reduction rate that the 6016 aluminum alloy sheets can withstand before fracture under plane strain. Measurement results are shown in Table 13, the average thickness at fracture of the PST-specimens ranged from 0.65 to 0.66mm.

6 Conclusions

The main objective of this study is to investigate the mechanical properties and forming characteristics of the 6016-T4 aluminum alloy sheets used for auto panels through tensile tests under different strain paths. Based on the aforementioned research, the following conclusions can be drawn:

(1) The 6016 aluminum alloy sheets have a small yield ratio and a large strain hardening index, with average values of 0.510 and 0.263 at different angles. Additionally, they can be considered isotropic in-plane, which is beneficial for forming. Pre-straining and baking can enhance their mechanical properties, with the degree of improvement increasing with higher levels of pre-strain.

(2) The saturated model represented by the Voce model is more suitable for the 6016 aluminum alloy sheets than the unsaturated model represented by the Hollomon model. Further improvement was made to the Voce model by enhancing it into the Voce + Voce model, which involved increasing the number of fitting coefficients to enhance the model's fitting performance.

(3) For the 1mm thick 6016 aluminum alloy sheets, under uniaxial tensile strain path, the average thickness at the onset of necking ranged from 0.80 to 0.85mm, while the average thickness at fracture ranged from 0.63 to 0.65mm. Under plane strain path, the average thickness at the onset of necking ranged from 0.79 to 0.81mm, and the average thickness at fracture ranged from 0.65 to 0.66mm.

Acknowledgements This work has been partially supported by the National Key Research and Development Program of China (2019YFA0708803) and the National Natural Science Foundation of China (Grant No. 52205487).

Author contribution All authors contributed to the study conception and design. Material preparation, data collection and analysis were performed by Ziyun Huang, Shuhui Li, Shun Liu and Sun Jin. The first draft of the manuscript was written by Ziyun Huang and all authors commented on previous versions of the manuscript. All authors read and approved the final manuscript.

Declarations

Conflict of interest The authors declare no competing interests.

References

1. Tisza M, Czinege I (2018) Comparative study of the application of steels and aluminium in lightweight production of automotive parts. Int J Light Mater Manuf 1(4):229–238. https://doi.org/10.1016/j.ijlmm.2018.09.001
2. Zhang W, Xu J (2022) Advanced lightweight materials for automobiles: a review. Materi Des 110994. https://doi.org/10.1016/j.matdes.2022.110994
3. Li M, Wang Y, Yang S, Tao W, Zhang G (2021) Improving mechanical properties and electrode life for joining aluminum alloys with innovatively designated Newton ring electrode. J Manuf Process 64:948–959. https://doi.org/10.1016/j.jmapro.2021.02.001
4. Ferreira V, Egizabal P, Popov V, de Cortázar MG, Irazustabarrena A, López-Sabirón AM, Ferreira G (2019) Lightweight automotive components based on nanodiamond-reinforced aluminium alloy: A technical and environmental evaluation. Diam Relat Mater 92:174–186. https://doi.org/10.1016/j.diamond.2018.12.015
5. Peppas A, Kollias K, Dragatogiannis DA, Charitidis CA (2021) Sustainability analysis of aluminium hot forming and quenching technology for lightweight vehicles manufacturing. Int J Thermofluids 10:100082. https://doi.org/10.1016/j.ijft.2021.100082
6. Abbasi M, Hamzeloo SR, Ketabchi M, Shafaat MA, Bagheri B (2014) Analytical method for prediction of weld line movement during stretch forming of tailor-welded blanks. Int J Adv Manuf Technol 73:999–1009. https://doi.org/10.1007/s00170-014-5850-3
7. Liu W, Peng T, Kishita Y, Umeda Y, Tang R, Tang W, Hu L (2021) Critical life cycle inventory for aluminum die casting: A lightweight-vehicle manufacturing enabling technology. Appl Energy 304:117814. https://doi.org/10.1016/j.apenergy.2021.117814
8. Atxaga G, Arroyo A, Canflanca B (2022) Hot stamping of aerospace aluminium alloys: Automotive technologies for the aeronautics industry. J Manuf Process 81:817–827. https://doi.org/10.1016/j.jmapro.2022.07.032
9. Cui M, Jo YH, Kim YW, Kim HW, Lee JH (2022) The effect of different preaging conditions on mechanical properties and clustering behavior of AA6016 sheets for automotive outer panels. J Market Res 20:238–245. https://doi.org/10.1016/j.jmrt.2022.07.043
10. Geng HC, Wang YL, Zhu B, Wang ZJ, Zhang YS (2022) Effect of solution treatment time on plasticity and ductile fracture of 7075 aluminum alloy sheet in hot stamping process. Trans Nonferrous Metals Soc China 32(11):3516–3533. https://doi.org/10.1016/S1003-6326(22)66036-9
11. Guo X, Xu H, Zeng Q, Pet T (2021) Springback characteristics of arched aluminum alloy gusset plate after stamping forming. Thin-Walled Structures 159:107294. https://doi.org/10.1016/j.tws.2020.107294
12. Wang C, Yi Y, Wang H, Dang J, An Q, Dong F, Chen M (2023) Investigation on the formability and deformation mechanism of aluminum alloy thin-walled parts at cryogenic temperature. J Mater Proc Technol 118041. https://doi.org/10.1016/j.jmatprotec.2023.118041
13. Hou H, Zhao G, Yu J, Sun Y, Li H (2023) Experimental studies and modeling of strain rate-and temperature-dependent springback behavior of hot-deformed aluminum alloys. J Mater Process Technol 318:118029. https://doi.org/10.1016/j.jmatprotec.2023.118029
14. Feng B, Gu B, Li S (2023) An efficient pre-hardened cryogenic forming process for AA7075 aluminum alloy sheets. J Manuf Process 92:534–547. https://doi.org/10.1016/j.jmapro.2023.02.061
15. Ambrogio G, Gagliardi F (2015) Temperature variation during high speed incremental forming on different lightweight alloys. Int J Adv Manuf Technol 76:1819–1825. https://doi.org/10.1007/s00170-014-6398-y
16. Chen MH, Gao L, Zuo DW, Wang M (2007) Application of the forming limit stress diagram to forming limit prediction for the multi-step forming of auto panels. J Mater Process Technol 187:173–177. https://doi.org/10.1016/j.jmatprotec.2006.11.178
17. Abbasi M, Bagheri B, Abdollahzadeh A, Moghaddam AO (2021) A different attempt to improve the formability of aluminum tailor welded blanks (TWB) produced by the FSW. IntJ Mater Form 14:1189–1208. https://doi.org/10.1007/s12289-021-01632-w
18. Li G, Deng H, Mao Y, Zhang X, Cui J (2018) Study on AA5182 aluminum sheet formability using combined quasi-static-dynamic tensile processes. J Mater Process Technol 255:373–386. https://doi.org/10.1016/j.jmatprotec.2017.12.038
19. Paul SK (2023) A physics-based defect tolerant design approach to predict the tensile performance of aluminium alloys with a defect. Theoret Appl Fract Mech 127:104033. https://doi.org/10.1016/j.tafmec.2023.104033
20. Rex AV, Paul SK, Singh A (2023) The influence of equi-biaxial and uniaxial tensile pre-strain on the low cycle fatigue performance of the AA2024-T4 aluminium alloy. Int J Fatigue 173:107699. https://doi.org/10.1016/j.ijfatigue.2023.107699
21. Neto DM, Simões VM, Oliveira MC, Alves JL, Laurent H, Oudriss A, Menezes LF (2020) Experimental and numerical analysis of the heat generated by plastic deformation in quasi-static uniaxial tensile tests. Mech Mater 146:103398. https://doi.org/10.1016/j.mechmat.2020.103398
22. Shen W, Xue F, Li C, Liu Y, Mo X, Gao Q (2023) Study on constitutive relationship of 6061 aluminum alloy based on Johnson-Cook model. Mater Today Commun 37:106982. https://doi.org/10.1016/j.mtcomm.2023.106982
23. Zhang R, Jiang J, Lin J, Yardley VA (2023) Investigation of variability in apparent values of materials properties in thermo-mechanical uniaxial tensile tests on sheet metals. J Manuf Process 101:737–754. https://doi.org/10.1016/j.jmapro.2023.06.005
24. Lu J, Song Y, Hua L, Zheng K, Dai D (2018) Thermal deformation behavior and processing maps of 7075 aluminum alloy sheet based on isothermal uniaxial tensile tests. J Alloy Compd 767:856–869. https://doi.org/10.1016/j.jallcom.2018.07.173
25. Xiao W, Wang B, Zheng K (2017) An experimental and numerical investigation on the formability of AA7075 sheet in hot stamping condition. Int J Adv Manuf Technol 92:3299–3309. https://doi.org/10.1007/s00170-017-0419-6
26 Yan JB, Kong G, Zhang L (2023) Low-temperature tensile behaviours of 6061–T6 aluminium alloy: Tests, analysis, and numerical simulation. Structures 56:105054. https://doi.org/10.1016/j.istruc.2023.105054. (Elsevier)
27. Bagheri B, Abbasi M, Hamzeloo R (2021) Comparison of different welding methods on mechanical properties and formability behaviors of tailor welded blanks (TWB) made from AA6061

alloys. Proc Inst Mech Eng C J Mech Eng Sci 235(12):2225–2237. https://doi.org/10.1177/0954406220952504
28. Thirathipviwat P, Nozawa S, Furusawa M, Onuki Y, Hasegawa M, Matsumoto K, Sato S (2023) A correlation between texture evolution and dislocation density in Al-Mg alloys during uniaxial tensile deformation. Mater Lett 134829. https://doi.org/10.1016/j.matlet.2023.134829
29. Wang Y, Huang Z, Zhu P, Zhu R, Hu T, Zhang D, Jiang D (2023) Effects of compressed speckle image on digital image correlation for vibration measurement. Measurement 217:113041. https://doi.org/10.1016/j.measurement.2023.113041
30. Preisler D, Knapek M, Harcuba P, Chráska T, Stráský J (2023) High-throughput evaluation of mechanical properties of biomedical Ti alloys by digital image correlation and acoustic emission. Mater Lett 351:135043. https://doi.org/10.1016/j.matlet.2023.135043
31. Zhou M, Li Y, Hu Q, Li X, Chen J (2019) Investigations on edge quality and its effect on tensile property and fracture patterns of QP980. J Manuf Process 37:509–518. https://doi.org/10.1016/j.jmapro.2018.12.028
32. Traphöner H, Clausmeyer T, Tekkaya AE (2021) Methods for measuring large shear strains in in-plane torsion tests. J Mater Process Technol 287:116516. https://doi.org/10.1016/j.jmatprotec.2019.116516
33. Deng H, Yang S, Li G, Zhang X, Cui J (2020) Novel method for testing the high strain rate tensile behavior of aluminum alloys. J Mater Process Technol 280:116601. https://doi.org/10.1016/j.jmatprotec.2020.116601
34. Liu C (2023) Evolution of deformation and stress during necking in uniaxial tension. Forces Mech 100201. https://doi.org/10.1016/j.finmec.2023.100201
35. Fang S, Zheng X, Guo B, Sia B, Yang L (2023) A new method for localized necking detection in uniaxial tensile testing based on a multi-camera DIC system. Mater Today Commun 35:106021. https://doi.org/10.1016/j.mtcomm.2023.106021
36. Jordan B, Grolleau V, Mohr D (2023) Using surround DIC to extract true stress–strain curve from uniaxial tension experiments. Int J Solids Struct 268:112171. https://doi.org/10.1016/j.ijsolstr.2023.112171
37. Li J, Yang G, Siebert T, Shi MF, Yang L (2018) A method of the direct measurement of the true stress–strain curve over a large strain range using multi-camera digital image correlation. Opt Lasers Eng 107:194–201. https://doi.org/10.1016/j.optlaseng.2018.03.029
38. Peirs J, Verleysen P, Degrieck J (2012) Novel technique for static and dynamic shear testing of Ti6Al4V sheet. Exp Mech 52:729–741. https://doi.org/10.1007/s11340-011-9541-9
39. Gonoring TB, de Miranda Salustre MG, Caetano GA, Martins JBR, Orlando MTDA (2022) A constitutive model for the uniaxial tensile plastic behavior of metals based on the instantaneous strain-hardening exponent. J Market Res 20:2421–2443. https://doi.org/10.1016/j.jmrt.2022.07.189
40. Marciniak Z, Duncan JL, Hu SJ (2002) Mechanics of sheet metal forming, 2nd edn. Butterworth Heinemann, Oxford
41. Li H, Yan Z, Cao L (2018) Bake hardening behavior and precipitation kinetic of a novel Al-Mg-Si-Cu aluminum alloy for lightweight automotive body. Mater Sci Eng, A 728:88–94. https://doi.org/10.1016/j.msea.2018.05.014
42. Yu J, Pang Q, Hu Z (2023) Effects of pre-stretching and baking treatment on microstructural evolution and mechanical properties of 7A09 aluminum alloy subjected to pre-hardening forming. J Alloys Compd 170915. https://doi.org/10.1016/j.jallcom.2023.170915
43. Hollomon JH (1945) Tensile deformation. Aime Trans 12(4):1–22
44. Voce E (1948) The relationship between stress and strain for homogeneous deformation. J Inst Met 74:537–562